AD-A105 865 NAVAL POSTGRADUATE SCHOOL MONTEREY CA F/G 17/5
STUDY OF THE PERFORMANCE PARAMETERS OF A FLIR SYSTEM.(U)
JUN 81 Y B LEE, C H PARK

UNCLASSIFIED NL

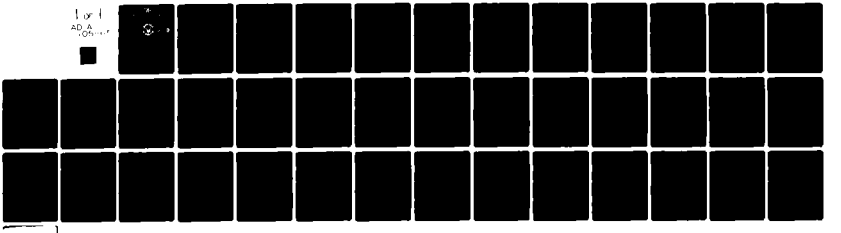

END
DATE FILMED
11-81
DTIC

LEVEL II

(2)

NAVAL POSTGRADUATE SCHOOL

Monterey, California

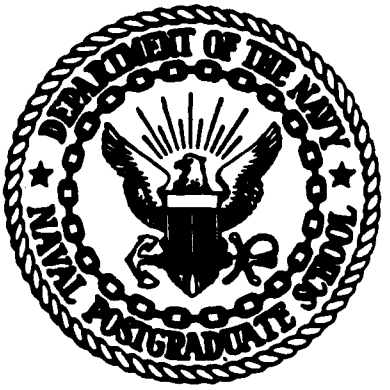

THESIS

STUDY OF THE PERFORMANCE PARAMETERS OF A FLIR SYSTEM

by

Yong Bok Lee
and
Chang Hyun Park

June 1981

Thesis Advisor: E. C. Crittenden

Approved for public release; distribution unlimited

SECURITY CLASSIFICATION OF THIS PAGE (When Data Entered)

REPORT DOCUMENTATION PAGE	READ INSTRUCTIONS BEFORE COMPLETING FORM
1. REPORT NUMBER	2. GOVT ACCESSION NO. AD-A105865	3. RECIPIENT'S CATALOG NUMBER
4. TITLE (and Subtitle) Study of the Performance Parameters of a FLIR Systems.	5. TYPE OF REPORT & PERIOD COVERED Master's Thesis June 1981
	6. PERFORMING ORG. REPORT NUMBER
7. AUTHOR(s) Yong Bok Lee and Chang Hyun Park	8. CONTRACT OR GRANT NUMBER(s)
9. PERFORMING ORGANIZATION NAME AND ADDRESS Naval Postgraduate School Monterey, California 93940	10. PROGRAM ELEMENT, PROJECT, TASK AREA & WORK UNIT NUMBERS
11. CONTROLLING OFFICE NAME AND ADDRESS Naval Postgraduate School Monterey, California 93940	12. REPORT DATE June 1981
	13. NUMBER OF PAGES 39
14. MONITORING AGENCY NAME & ADDRESS (if different from Controlling Office)	15. SECURITY CLASS. (of this report) UNCLASSIFIED
	15a. DECLASSIFICATION/DOWNGRADING SCHEDULE

16. DISTRIBUTION STATEMENT (of this Report)

Approved for public release; distribution unlimited

17. DISTRIBUTION STATEMENT (of the abstract entered in Block 20, if different from Report)

18. SUPPLEMENTARY NOTES

19. KEY WORDS (Continue on reverse side if necessary and identify by block number)

NPS FLIR, Thermal Imaging, IR Imaging Performance Parameters

20. ABSTRACT (Continue on reverse side if necessary and identify by block number)

The performance parameters of Detectivity and Noise Equivalent Temperature Difference for a Forward Looking Infra-Red (FLIR) system were measured after optimization of the system. The achieved performance approached the theoretically evaluated limiting values.

DD FORM 1 JAN 73 1473 (Page 1) EDITION OF 1 NOV 65 IS OBSOLETE S/N 0102-014-6601

251450

SECURITY CLASSIFICATION OF THIS PAGE (When Data Entered)

Approved for public release; distribution unlimited

Study for the Performance Parameters of a FLIR System

by

Yong Bok Lee
Lieutenant Colonel, Republic of Korea Army
B.S., Korean Military Academy, 1966

Chang Hyun Park
Lieutenant Colonel, Republic of Korea Army
B.S., Korean Military Academy, 1965

Submitted in partial fulfillment of the requirements for the degree of

MASTER OF SCIENCE IN PHYSICS

from the

NAVAL POSTGRADUATE SCHOOL
June 1981

Author: Park Chang Hyun
Lee, Yong Bok

Approved by: E. R. Crittenden Jr.
Thesis advisor
Edmund A. Milne
Second Reader
J. M. Dyer
Chairman, Department of Physics and Chemistry
William M. Tolles
Dean of Science and Engineering

ABSTRACT

The performance parameters of Detectivity and Noise Equivalent Temperature Difference for a Forward Looking Infra-Red (FLIR) system were measured after optimization of the system. The achieved performance approached the theoretically evaluated limiting values.

TABLE OF CONTENTS

LIST OF FIGURES

ACKNOWLEDGEMENT

We wish to express our appreciation to Professor Milne for his assistance and we wish to acknowledge the assistance of Mr. Bob Moeller and Mr. Ken Smith with the mechanical structure and electronic equipment.

We would like to especially thank Professor Eugene Crittenden whose wisdom and guidance were invaluable in preparation of this thesis.

Finally, we would like to express our grateful thanks to all Professors of the Physics Department.

I. INTRODUCTION

A. BACKGROUND

Thermal imaging systems are of recent origin. Since the first real-time FLIR was possible in late 1960, the development of the thermal imaging system has been very rapid in its design and technology. It was the direct result of the rapid development of various types of detectors. The superiority in performance in all-weather conditions, and at night made its application wider than expected.

FLIR sensor technology is making significant strides that could earn indispensable roles for these real-time, 24 hour sensors in future aircraft, remotely piloted vehicles (RPV), missiles and air defense systems. Even the immediate prospects for wider deployment of FLIR sensors could hinge on the recent efforts to reduce the cost, size, weight and complexity of the real-time imaging devices. Some types are in the testing phase in ASW, TRAM (Target Recognition Attack Multisensor) and Attack aircraft.

To provide a basis for better understanding of FLIR systems, a basic type of FLIR system was assembled. The several performance parameters were measured, but these values were at first, in poor agreement with the theoretical values. The principal effort has been in bringing theoretical and experimental values into agreement.

B. OBJECTIVE

This paper is a brief review of the basic principles of operation and the performance parameter characteristics. Emphasis is placed on the measurement of D* (Specific Detectivity) and the direct evaluation of NETD (Noise Equivalent Temperature Different) in terms of D*.

The main scope of this study is in matching the measured and theoretically calculated NETD values. For this purpose the whole system was re-examined and several new experimental devices have been designed and constructed.

II. THEORY

A. SYSTEM PRINCIPLES

FLIR, Forward Looking Infra-Red, is a thermal imaging system which produces an image, primarily by self emission of a target and by the target's emissivity difference in the Infra-Red wavelength region.

The thermal radiation from a target in the IR region, 8-14 μm, has good atmospheric transmission and also corresponds to the peak thermal radiation from an object at ambient temperature. The radiation is collected and focused onto an IR detector by an optical system. The impinging radiation on the detector excites charge carriers across the bandgap of a semiconductor.

For quantum detectors like HgCdTe, one excess electron-hole pair is created for each photon absorbed. For a photoconductive detector as used here, this changes the conductivity of the material. Since the attached circuit provides a constant current through the material; the voltage drop across the detector varies inversely with the incident radiation intensity. Naturally there is a lower limit to the photon energy below which the detector will not respond. The lower limit is the direct energy bandgap E_g and the wavelength corresponding to this lower photon energy limit is called the cut-off wavelength.

The detector converts the optical signal intensity into the analog electrical signal. This is then amplified and processed for display on a video monitor. One can reproduce the image of a target which generates Infra-Red thermal radiation even in the absence of ambient light. The whole system is described simply by the block diagram shown in Figure 1.

B. SYSTEM PARAMETERS

Several detector and system parameters are used to describe the system performance. These are R, D*, NEP, NETD, MRTD and MDTD, which individually represent; Responsivity, Specific Detectivity, Noise Equivalent Power, Noise Equivalent Temperature Difference, Minimum Resolvable Temperature Difference, and Minimum Detectable Temperature Difference. Some of the important parameters among these usually have the definition and expression given below.

1. NEP

Noise Equivalent Power (NEP) is defined as the signal power which produces a Signal-to-Noise ratio of unity.

$$NEP = \frac{P_d}{(V_s/V_n)} \quad [watt] \qquad (1)$$

where P_d [watt] : signal power incident on the detector sensitive area, same as $H_d A_d$

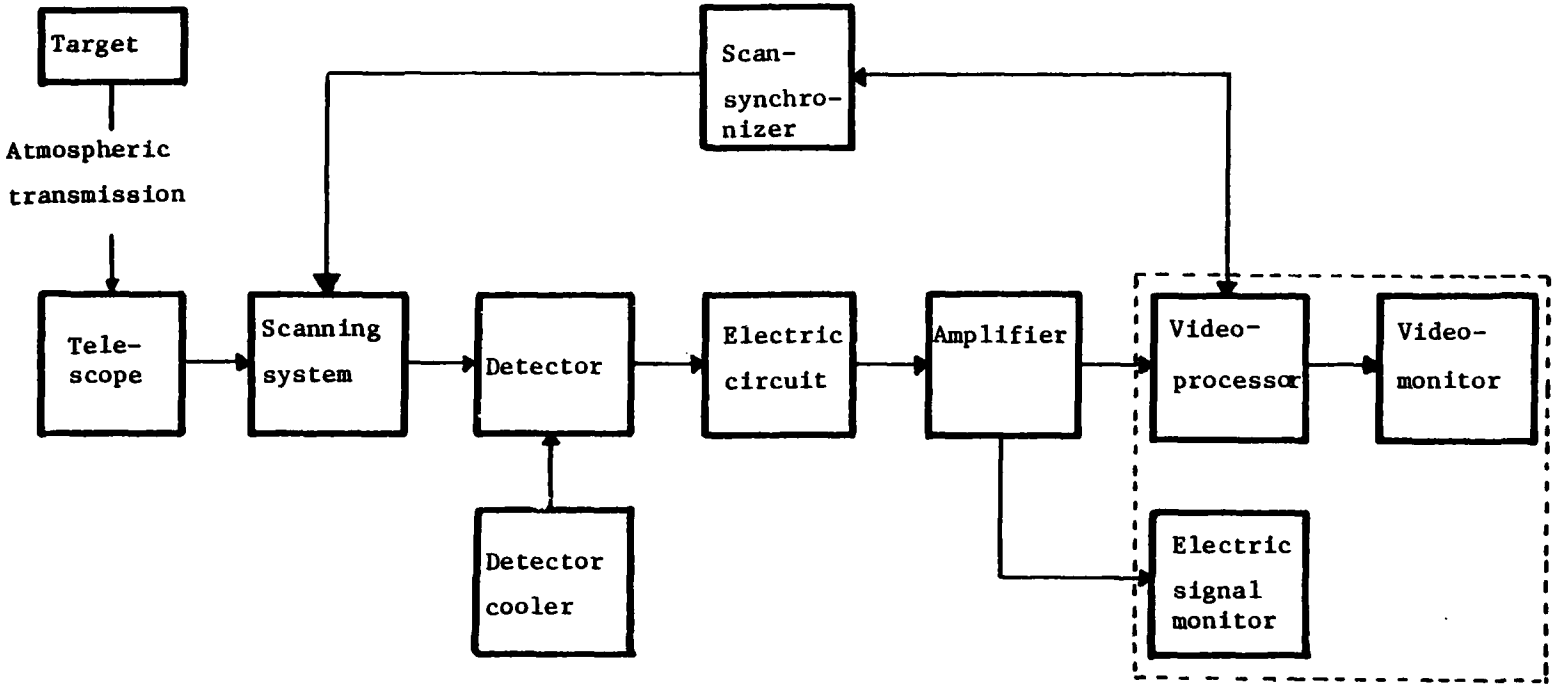

FIG. 1 FLIR system

H_d [watt/cm^2] : irradiance on the detector

A_d [cm^2] : detector sensitive area

(V_s/V_n) : signal-to-noise voltage ratio

2. D*

Specific Detectivity (D*) is a detector performance parameter which represents the detector output signal-to-noise ratio for one watt of input signal power for a unit detector area and a unit electrical bandwidth.

$$D^*(\lambda,f) = \frac{(A_d\,\Delta f)^{1/2}}{H_d\,A_d}\,(V_s/V_n) \qquad (2)$$

where

Δf [Hz] : system bandwidth

V_n [volts] : detector rms noise voltage measured in the bandwidth of Δf.

V_s [volts] : detector signal voltage as a function of wavelength and electrical frequency.

D* comes from the expression of D (Detectivity) which is the reciprocal of NEP.

The assumptions made in the process of derivation require that detector noise varies as $A_d^{1/2}$ and $\Delta f^{1/2}$, [Ref. 1]. The first assumption is valid for photon detectors as long as the detector areas do not vary by more than an order of magnitude. The second approximation requires either that noise is frequency invariant over the amplifier bandwidth, or that it is measured over such a narrow band that a

variation is insignificant. Further details can be found in Lloyd. [Ref. 2].

3. NETD

Noise Equivalent Temperature Difference (NETD) is a measure of the ability of a system to discriminate small signals in the presence of noise. NETD is defined as the blackbody target-to-background temperature difference in a standard test pattern which produces a peak signal-to-rms noise ratio of unity when the system views the test pattern. [Ref. 2]. This is given as

$$NETD = \frac{\Delta T}{(V_s/V_n)} \tag{3}$$

where

ΔT [^{o}K] : temperature difference between a target and background

NETD is also theoretically derived by Lloyd [Ref. 2] as

$$NETD = \frac{\pi (A_d \, \Delta f)^{\frac{1}{2}}}{\alpha\beta A_c \int_o^\infty \frac{\partial W}{\partial t} \, D^*(\lambda) \, \tau_o(\lambda) \, d\lambda} \tag{4}$$

where

α,β : detector angular subtense which is $\alpha = a/f$, $\beta = b/f$ where a,b are the size of a rectangular detector cell and f is the focal length of the optic system.

$\tau_o(\lambda)$: IR optical transmission as a function of wavelength.

W_λ [watt/cm^2] : radiant emmitance of a target

For some systems it is possible to assume that $\tau_o(\lambda)$ = const. within specific wavelength region $\lambda_1 \leq \lambda \leq \lambda_2$ and $\tau_o(\lambda) = 0$ elsewhere.

Then

$$NETD = \frac{(A_d \, \Delta f)^{\frac{1}{2}}}{\alpha\beta \, A_o \tau_o} \frac{1}{\int_{\lambda_1}^{\lambda_2} \frac{\partial W_\lambda(T)}{\partial T} D^*(\lambda) \, d\lambda} \tag{5}$$

4. MRTD

Minimum Resolvable Temperature Difference (MRTD) is defined as the image signal-to-noise ratio required for an observer to resolve an equally spaced four bar target that is obscured by noise. MRTD is also derived by Lloyd [Ref. 2] under several assumptions.

$$MRTD = \frac{3 \, (NETD/\Delta f) \, f_T \, (\alpha\beta)^{\frac{1}{2}} / \tau d}{r_s \, (T_e \, \dot{F})^{\frac{1}{2}}} \tag{6}$$

where

f_T	[H_z/mrad]	:	fundamental target frequency
T_e	[sec]	:	effective eye integration time
τd	[sec]	:	detector dwell time
$\dot{F}$	[H_z]	:	frame rate
r_s		:	overall system MTF

5. MDTD

Minimum Detectable Temperature Difference (MDTD) is the blackbody temperature difference required for an

observer to detect the presence of a square target when he is allowed unlimited time to make a decision and knows where to look for the target. Lloyd derived the expression of MDTD under the same assumption as MRTD.

$$MDTD = \frac{r_s \; 1.5 \sqrt{2} MRTD \; (f_T - 1/2w)}{\overline{I\;(x,y)}} \qquad (7)$$

where

$\overline{I(x,y)}$: average value of the convolution integral of the image of the square target

The derivations for the NETD, MRTD, and MDTD are carried out in detail with all assumptions in Lloyd [Ref. 2], so the derivations are omitted here.

The parameters, MRTD and MDTD, have important meaning in expressing the ability of the human eye to resolve or detect the target image on the video monitor. However, this is not a key point in this study.

D* and NETD are by far the most frequently used figures of merit for characterizing the sensitivity of Infra-Red quantum detectors and FLIR systems. Since those two parameters are considered the most basic and fundamental parameters, further study of these was carried out.

C. DIRECT EVALUATION OF NETD IN TERMS OF D*

In order to compare measured and theoretical values of NETD, a form is needed which permits use of directly measured quantities. Calculation of the theoretical

value of NETD by the expression from Lloyd is a time consuming job. It also requires knowledge of the spectral variation of D*, not available without additional equipment which is not presently available. A more convenient form of this parameter expression is developed as follows.

1. Derivation of D*

Basically the expression for Specific Detectivity is developed for the ultimate derivation of NETD expression rather than for itself. To derive a new expression of D* one can imagine a simple experiment set-up as shown in Figure 2.

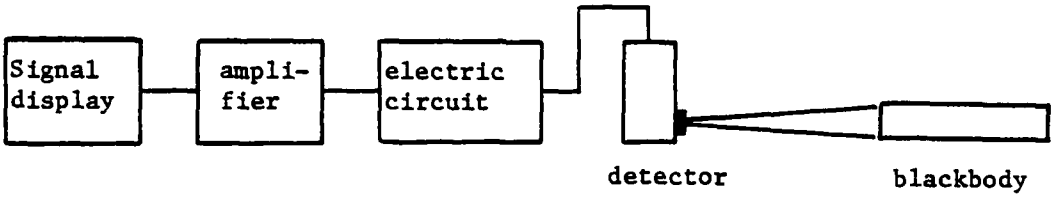

Fig. 2 Experiment set-up for detectivity derivation.

Total irradiance at the blackbody [watt]: $H_s A_s$

where

H_s [watt/cm^2] : irradiance of the blackbody

A_s [cm^2] : area of blackbody perpendicular to the line of sight

Total irradiance at the blackbody per steradian

$$[\text{watt}/S_r] \quad : \quad H_s A_s/\pi$$

Detector area expressed in terms of solid angle S_r: A_d/Z^2 where Z [cm] : distance between detector and blackbody

Total power absorbed into detector P_d

$$P_d \text{ [watt]} = (A_d/Z^2)\ (H_s A_s/\pi) \tag{8}$$

General expression of D*

$$D^* \text{ [cm } H_z^{\frac{1}{2}}/\text{watt]} = \frac{(A_d \Delta f)^{\frac{1}{2}}}{P_d}\ (V_s/V_n)$$

$$D^* = \frac{(A_d \Delta f)^{\frac{1}{2}}\ Z^2 \pi\ (V_s/V_n)}{A_d A_s\ H_s} \tag{9}$$

All terms in the expression for D* in equation (9) can be directly read or measured in the experimental process.

2. Derivation of NETD

The expression for NETD, directly based on the defintion of it, provides a good starting point to derive a more convenient form. This also leads to a form capable of direct experimental verification.

$$\text{NETD} = \frac{\Delta T}{(V_s/V_n)} \tag{10}$$

Figure 3 shows the simplified optical system, target and detector excluding all of the electronic elements. A pinhole (Area A_p) is also attached to provide an ability to improve the spatial resolution.

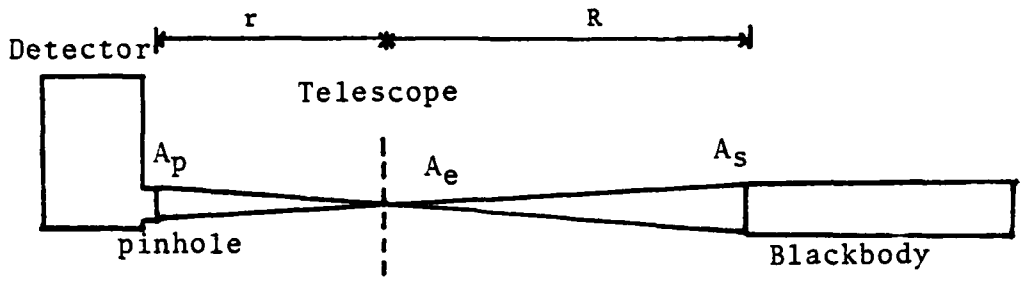

Fig. 3 Experiment set-up for NETD Derivation

Power absorbed by the detector $P_d = A_e H_s A_s / R^2$ where R is the distance between the telescope primary mirror and a target

Optics f/# = r/D = N

where D is a diameter of primary mirror

Area of primary mirror: A_e [cm^2]

Irradiance of blackbody surface: H_s [watt/cm^2] = $G_s \Delta T$

where G_s is a proportionality coefficient

Then,

$$P_d = (1/R^2)\ (1/4)\ \pi\ (r/N)^2\ (A_s/\pi)\ G_t \Delta T \qquad (11)$$

where $\Delta T = 4N^2 P_d / A_p G_t$

From Equation (2), (9), (10), (11)

$$\text{NETD} = \frac{4N^2}{A_p G_t} (A_d \Delta f)^{\frac{1}{2}}\ A_d A_s G_s \Delta T / (A_d \Delta f)^{\frac{1}{2}}\ Z^2\ (V_s/V_n)$$

Finally we can get a much more convenient form of NETD, that does not involve specifying the wavelength limits.

$$NETD = \frac{4N^2 A_d A_s}{\pi A_p Z^2}(V_n/V_s)\Delta T \qquad (12)$$

where $G_s/G_t = 1$ if one keeps consistency in temperature. All terms appearing in this expression for NETD in Equation (12) can be directly read or measured experimentally. It is clear from the Equation (12) that if ΔT is kept constant then NETD depends only on the pinhole size.

III. EXPERIMENTAL PROCEDURE AND MEASUREMENT

A. APPARATUS USED FOR EVALUATION

The FLIR system to be evaluated is a HgCdTe single cell, mechanically scanning thermal imaging system assembled at NAVPGSCOL. Since a former study [Ref. 3] described precisely the whole system, only the main feature of elements are briefly discussed here.

1. Optics; Cassegranian Type Dahl-Kirkham Telescope

   a. Diameter (D) : 15.24 cm

   b. Focal Length (f) : 228.6 cm

   c. Total Collecting Area : 172.8 cm^2

   d. To see the effect of the pinhole on the value NETD, an assembly of field lens and a pinhole are located in front of the detector.

   e. Scanning mechanism which consists of 2 mirrors mutually perpindicular to each other is mounted at an angle of 45^o to the beam exiting to the back end of the telescope. The scanning system could be located close to the exit aperture which means that it can be operating in the region where the image beam is parallel. The fact that a convergent beam scanner might cause the image deformation by mirror induced focal point shifting can be compensated. Because of the necessity for small mirror motion and the long focal length, the use of the convergent beam scanning technique

would not cause unacceptable image blur through beam focus.

2. Detector

a. Mercury Cadmium Teluride single cell detector with an IRTRAN-2 window operates in the 8-14 μm wavelength region.

b. A detector cell is mounted in a side-looking dewar and utilizes liquid nitrogen cooling down to 77 °K and is evacuated to 2×10^{-6} Torr.

c. The spectral response of the detector depends on the composition of the alloy and a wide range of performance is shown in Figure 4 from the supplier's specification [Ref. 4].

d. Manufacturer: Santa Barbara Research Center

e. Precise characteristics like Relative Responsivity vs. wavelength, Detectivity vs. Frequency, Responsivity vs. Frequency, Detectivity vs. Temperature can be referred to SBRC. [Ref. 4].

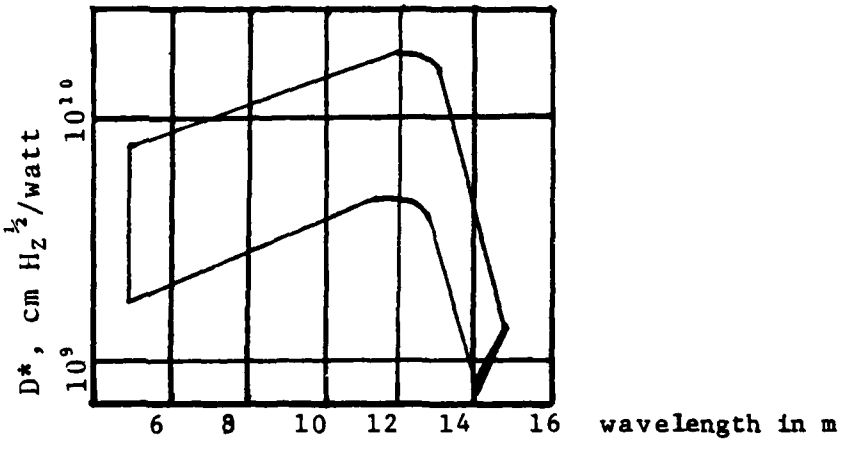

Fig. 4 Range of spectral detectivity

3. Blackbody Heat Source

A blackbody heat source is required for measuring the D* and NETD. Initially a U-shaped heating element with a long aluminum bar was used as a blackbody with a powerstat to control the temperature of the heating element. But it was not good enough as a blackbody target due to the low emissivity of the target and very fast heat dissipation and severe fluctuation of temperature due to the ambient background.

So, a new blackbody target covered with asbestos and fiber glass as an insulator to prevent heat loss into the ambient background, was designed and built as shown in Figure 5.

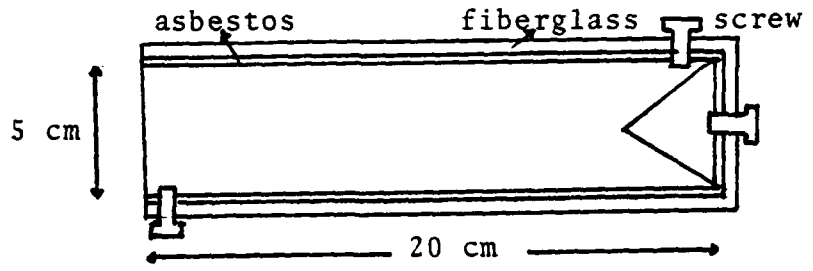

Fig. 5 Blackbody Heat Source

The cone inside this aluminum cylinder is used to increase internal reflections. Three screws at three different places are used to connect the thermocouples. A thermocouple attached to this blackbody heat source is used to measure the temperature with an accuracy of ± 0.1 °C.

4. Electronic Equipment

The electronic equipment is described in detail in the former study. [Ref. 5] . A brief summary of the equipment follows:

a. Hewlett Packard 3310 A Function Generator
: Raster control

b. General Scanning CCX 101 scanner control
: mirror drive

c. Wavetek 180 Function Generator
: Raster control

d. Princeton Applied Research Model 113 Preamplifier
: detector signal amplifier

e. Hewlett Packard 3400A RMS Voltmeter
: noise voltage measurement

f. Monsanto AM-6419/USM-368 OSC.
: display

Since HgCdTe is used as a photoconductor, a special electric circuit is needed to provide the conduction current. Figure 6 shows this electric circuit.

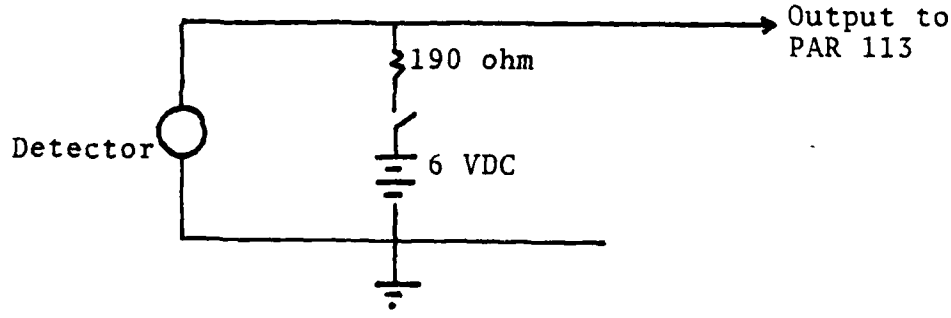

Fig. 6 Electric Circuit

B. MEASUREMENT AND CALCULATION

1. D*

To determine the detectivity it is necessary to measure the signal-to-noise voltage ratio. For this purpose a simple experiment is set up as shown in Figure 7.

Since the detector can detect only a change of radiation, a chopper is used to convert the steady radiation from the blackbody heat source into intermittent radiation. An aluminum plate, which has a hole in it, and is insulated with asbestos and fiber glass on both sides to prevent any thermal effect from the chopper or from any other heat source except blackbody heat source itself, is used as a real blackbody target. The fact that this aluminum plate with a hole, not the blackbody heat source, acts as a real blackbody can be easily verified by observing that the signal voltage is dependent on the distance between the aluminum plate and the detector, not on the distance from the detector to the blackbody heat source.

$\Delta f = 3000\ H_z$

$A_d = 0.04\ cm^2$

$A_s = \pi\ cm^2$

$Z = 50\ cm$

$H_s = 0.059\ watt/cm^2$ using calculator program [Appendix] where the inputs are

$\lambda_1 = 8\ \mu m$

$\lambda_2 = 14\ \mu m$

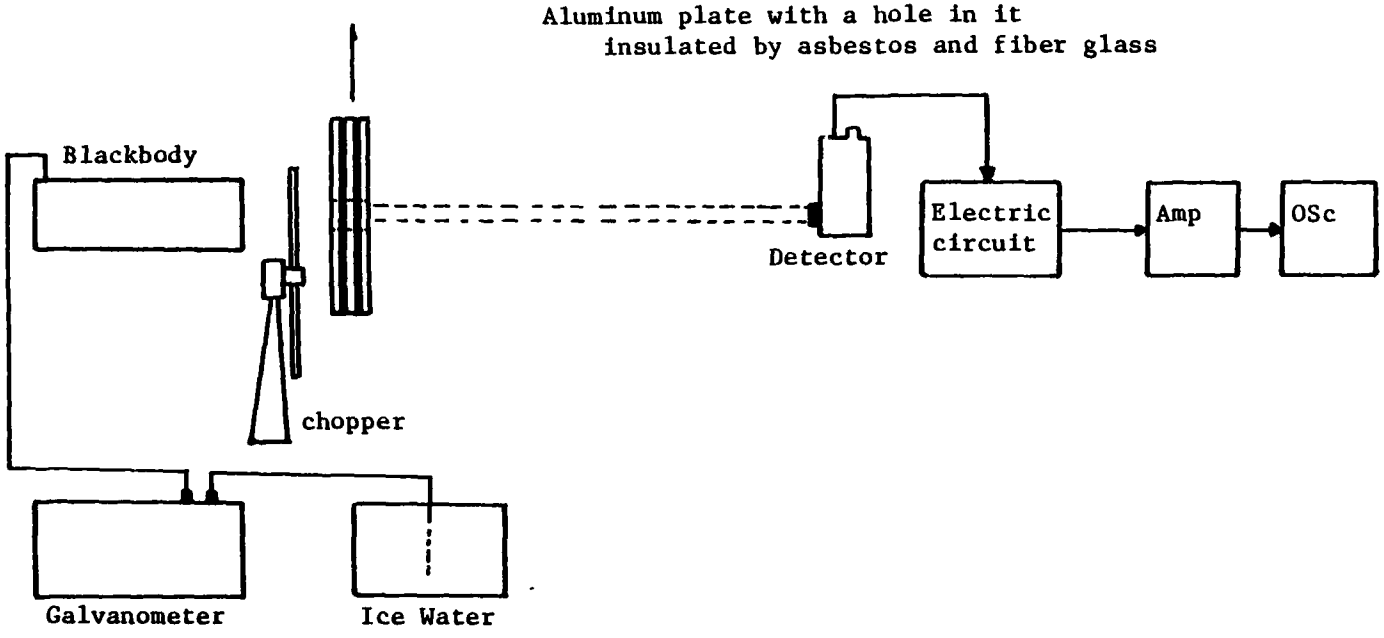

Fig. 7 Detectivity measurement experiment set-up

T_t = 163 °C (Blackbody Temperature)

T_b = 22 °C (Background Temperature)

V_s/V_n = 400 where measured value of

V_s = 0.6 volts (Reading from the Oscilloscope)

V_n = 0.0015 (System Noise Voltage, reading from the rms Noise voltage meter)

Calculation of D* using the previously derived detectivity expression, Equation (9) yields

$$D^* = 0.46 \times 10^{10} [cmHz^{\frac{1}{2}}/watt]$$

This value is the lower limit of detectivity in Figure 5 where the values are from the SBRC. [Ref. 4].

2. NETD

The experimental NETD can be measured, using the FLIR system under the same condition of blackbody temperature as for the D* measurement by measuring the signal-to-noise voltage ratio for each size of pinhole. In this step it is important to ensure that the signal on the oscilloscope comes from the target, and not from any reflection.

The first thing to be checked was the shape of the image formed at the back focal point. An incandescent light bulb was used as a target at a long distance so that the incident light is considered as a parallel beam. Then, the image should be round and clear.

Secondly, the shape of a signal on the oscilloscope should have a flat top while turning the telescope

horizontally. This is based on the linear filter theory which map object distributions into image distributions by the process of convolution. This theory says that the image function is a weighted sum of the system response to the component delta functions of the object.

Every part of the system which might cause an image degradation due to the poor alignment and the reflection by system itself was checked. This procedure included checking the relative angle of the reflecting mirror to the beam exit from the telescope, the exact location of the pinhole at the back focal point, and the adjustment of the field lens assembly. Also an effort was made to keep the direction of the telescope scanning across the objective screen and the axis of the field lens-detector assembly on a horizontal path line.

Difficulty in keeping the target temperature constant was solved by using a newly designed blackbody heat source shown in Figure 5.

The chromel-alumel thermocouple was used with its reference junction in ice water.

Table 1 shows the measured signal and noise voltages and the calculated NETD based on this measurement using the Equation (3).

D of pinhole (cm)	V_s volts	V_n volts	V_S/V_n	NETD
0.0368	0.05	0.0015	33.3	4.23
0.05	0.09	"	60.0	2.35
0.75	0.135	"	90.0	1.57
0.1	0.188	"	125.3	1.12
0.15	0.241	"	160.7	0.87
no pinhole	0.38	0.0021	180.9	0.78

Table 1 NETD - Experimental Value

IV. ANALYSIS

Table 2 shows the theoretically calculated NETD and also the experimentally measured value as a function of pinhole size.

D. of pinhole	NETD		difference
	theoretical	experimental	
0.0368	3.77	4.23	0.46
0.05	2.04	2.35	0.31
0.075	0.91	1.67	0.76
0.1	0.51	1.12	0.61
0.15	0.23	0.87	0.64
no pinhole	0.1	0.78	0.68

Table 2 NETD - Theoretical and Experimental Value

The data of Table 2 are plotted in Figure 8. For reference, those values of NETD, measured and calculated in the former study [Ref. 5] are also included in Figure 8.

An analysis of the values of the performance parameter, NETD, in the table above, reveals several important points.

The experimentally measured values of the NETD are in reasonable agreement with the theoretical values calculated with Equation (11). Even though the difference is small enough, this discrepancy is understood as that, first, the temperature difference ΔT still fluctuates on a certain scale which affects the measured signal-to-noise ratio.

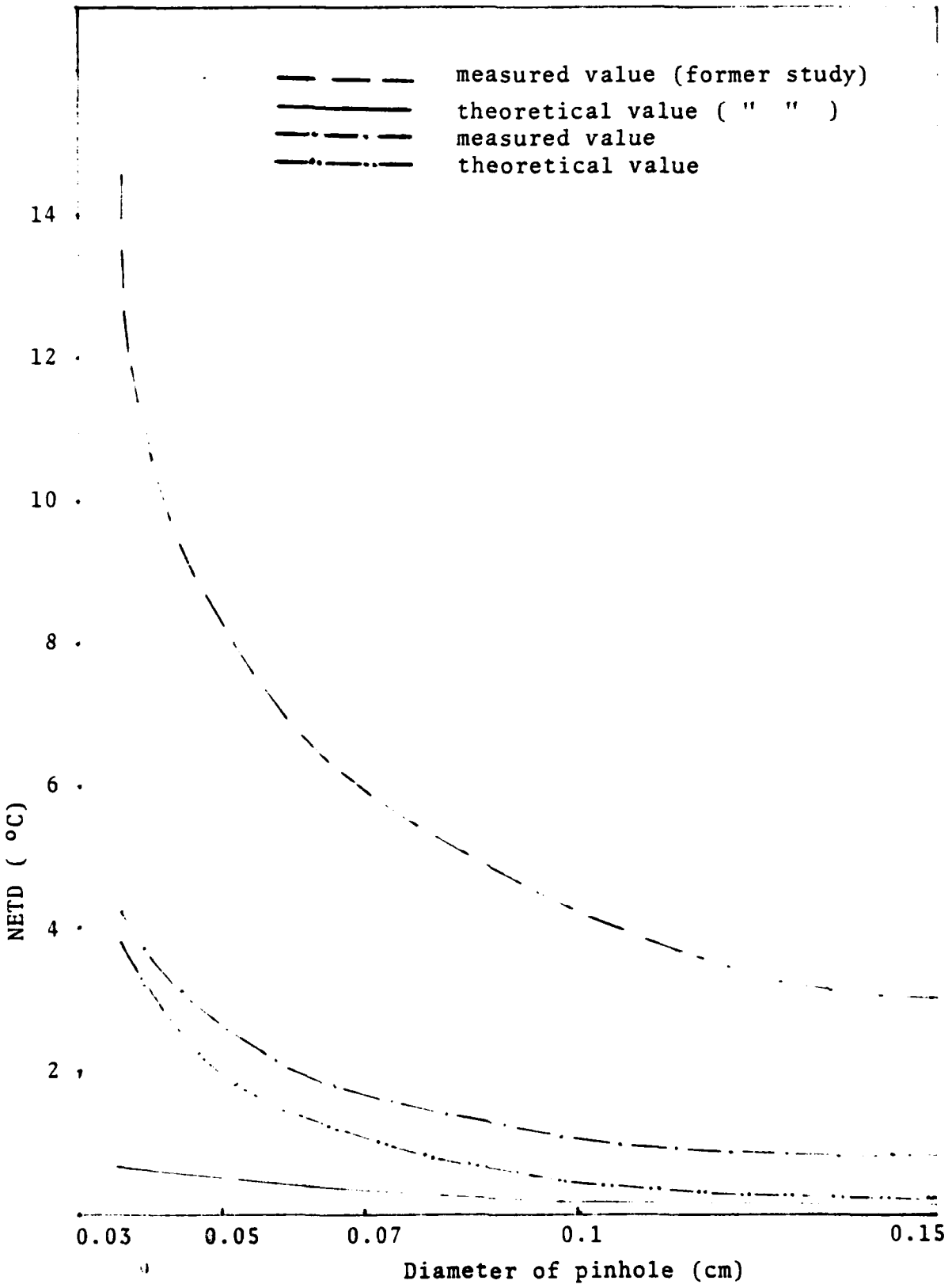

Fig. 8 NETD Comparison - theoretical and measured value

The temperature difference between the front end and back end of the blackbody furnace was 15 °C at the target temperature of 163 °C and ambient background temperature 22 °C. Considering that the approximate rate of change NETD with respect to the temperature difference (d NETD/dT) is about 0.02, the nonuniformity of the blackbody heat source can cause error in the NETD of 0.3 °C, which is half of the NETD difference in Table 2.

Second, this experiment basically assumed background limited noise conditions. But there should be another kind of noise, for example, 1/f noise.

Third, the alignment problem is another factor decreasing the accuracy of the measured experimental value. Using the more precise way of aligning, the result is believed to be much better.

The expected dependency of the thermal sensitivity of the system expressed by NETD upon the various size of pinhole was well observed. As expected, as the pinhole size gets larger, the system shows more sensitive response to the thermal radiation. The smaller size of the pinhole shows better resolution. Consequently, when all of the other factors like T, f/# are fixed, the NETD is a function cnly of area of the pinhole. This relation is well shown in Figure 8.

V. CONCLUSIONS

One of the basic performance parameters of the FLIR system, the NETD, was measured. Every effort was made to match the theoretical values and the experimentally measured values. For that purpose, a more convenient and direct form of NETD expression was derived. A new blackbody heat source was designed to more closely approximate a true blackbody. Most of the laboratory effort was spent in establishing precise optical alignment and in keeping the target and the background temperature difference constant. As a consequence the discrepancy between the theoretical and experimental values of NETD decreased to 0.3-0.7 °C, close enough to be considered in agreement. The result of measuring and calculating the NETD for 5 different sizes of pinholes show the variation of NETD with the pinhole size to be as theoretically anticipated.

As a secondary objective, the detectivity was measured and found to be 0.46×10^{10} cm $Hz^{\frac{1}{2}}$/watt. This value is the lower limit of detectivity in the characteristics provided by the detector manufacturer. Even though the value of D* is somewhat lower than expected, it can be understood to be a quality decrease due to a long term use, and one can say that D* is still in a tolerable region.

APPENDIX

CALCULATING "IN BAND" FLUX DENSITY OF BLACKBODY SOURCES USING TI-59

To use: press RST

enter λ_1 microns R/S

enter λ_2 " R/S

enter T A for °K

B for °F

C for °C

enter number of intervals

D for watt/cm^2

E for photons/sec/cm^2

000	42	STO	021	00	00	041	69	OP
001	01	01	022	69	OP	042	06	06
002	99	PRT	023	06	06	043	69	OP
003	91	R/S	024	69	OP	044	00	00
004	42	STO	025	00	00	045	75	-
005	02	02	026	91	R/S	046	03	3
006	99	PRT	027	76	LBL	047	02	2
007	91	R/S	028	12	B	048	95	=
008	76	LBL	029	42	STO	049	65	x
009	11	A	030	00	00	050	05	5
010	42	STO	031	02	2	051	55	÷
011	00	00	032	01	1	052	09	9
012	02	2	033	00	0	053	85	+
013	06	6	034	00	0	054	02	2
014	00	0	035	00	0	055	07	7
015	00	0	036	00	0	056	03	3
016	00	0	037	69	OP	057	95	=
017	00	0	038	04	04	058	42	STO
018	69	OP	039	43	RCL	059	00	00
019	04	04	040	00	00	060	91	R/S
020	43	RCL						

061	76	LBL
062	13	C
063	42	STO
064	00	00
065	01	1
066	05	5
067	00	0
068	00	0
069	00	0
070	00	0
071	69	op
072	04	04
073	43	RCL
074	00	00
075	69	OP
076	06	06
077	69	OP
078	00	00
079	43	RCL
080	00	00
081	85	+
082	02	2
083	07	7
084	03	3
085	95	=
086	42	STO
087	00	00
088	91	R/S
089	76	LBL
090	16	A'
091	42	STO
092	07	07
093	53	(
094	53	(
095	43	RCL
096	07	07
097	45	Y^x
098	43	RCL
099	09	09
100	65	x
101	53	(
102	53	(
103	43	RCL
104	06	06
105	45	Y^x
106	53	(
107	01	1
108	04	4
109	03	3
110	08	8
111	08	8
112	93	.
113	03	3
114	02	2
115	03	3
116	03	3
117	04	4
118	55	÷
119	43	RCL
120	07	7
121	55	÷
122	43	RCL
123	00	00
124	54	)
125	54	)
126	75	-
127	01	1
128	54	)
129	54	)
130	35	1/X
131	65	x
132	43	RCL
133	08	08
134	54	)
135	92	RTN
136	76	LBL
137	14	D
138	98	ADV
139	42	STO
140	05	05
141	99	PRT
142	98	ADV
143	53	(
144	43	RCL
145	02	02
146	75	-
147	43	rcl
148	01	01
149	54	)
150	55	÷
151	43	RCL
152	05	05
153	95	=
154	42	STO
155	03	03
156	03	3
157	93	.
158	07	7
159	04	4
160	01	1
161	01	1
162	00	0
163	07	7
164	04	4
165	52	EE
166	04	4
167	42	STO
168	08	08
169	95	5
170	42	STO
171	09	09
172	01	1
173	22	INV
174	23	LNX
175	42	STO
176	06	06
177	36	PGM
178	09	09
179	14	D
180	22	INV
181	52	EE
182	99	PRT
183	98	ADV
184	91	R/S
185	76	LBL
186	15	3
187	98	ADV
188	42	STO
189	05	05
190	99	PRT
191	98	ADV
192	53	(
193	43	RCL
194	02	02
195	75	-
196	43	RCL
197	01	01
198	54	)
199	55	÷
200	43	RCL
201	05	05
202	95	=
203	42	STO
204	03	03
205	01	1
206	93	.
207	08	8
208	08	8
209	03	3
210	06	6

211	05	5
212	01	1
213	06	6
214	52	EE
215	02	2
216	03	3
217	42	STO
218	08	08
219	04	4
220	42	STO
221	09	09
222	01	1
223	22	INV
224	23	LNX
225	42	STO
226	06	06
227	36	PGM
228	09	09
229	14	D
230	22	INV
231	52	EE
232	99	PRT
233	98	ADV
234	91	R/S

LIST OF REFERENCES

1. Levinstein, H., "State of the Art of Infrared Detector", Modern Utilization of Infrared Technology (III), SPIE, Vol. 124, 1977.

2. Lloyd, J. M., Thermal Imaging System, Plenum Press, 1975.

3. Gruber, J.P., Experimental FLIR Study, M.S. Thesis, Naval Postgraduate School, Monterey, California, 1979.

4. The SBRC Brochure, Santa Barbara Research Center, 1975.

5. Sellers, W. L., Measurements of Performance Parameters for a FLIR Thermal Imaging System, M.S. Thesis, Naval Postgraduate School, Monterey, California, 1980.

BIBLIOGRAPHY

Hudson, R.D., Infra-Red System Engineering, Wiley, 1969.

Kunz, C. A., Jr., Properties of Detectors for Infrared Transmitting Measurements, M.S. Thesis, Naval Postgraduate School, Monterey, California, 1974.

Miller, B., "FLIR Gaining Wider Service Acceptance", Aviation Week and Technology, May 7, 1973.

Miller, B., "Cost Reductions Key to Wider FLIR Use", Aviation Week and Technology, May 21, 1973.

Reine, M.B. and Broudy, R.M., "A Review of HgCdTe Infrared Detector", Modern Utilization of Infrared Technology III, SPIE, Vol. 124, 1977.

INITIAL DISTRIBUTION LIST

		No. Copies
1.	Defense Technical Information Center Cameron Station Alexandria, Virginia 22314	2
2.	Library, Code 0142 Naval Postgraduate School Monterey, California 93940	2
3.	Department Chairman, Code 61 Department of Physics & Chemistry Naval Postgraduate School Monterey, California 93940	2
4.	Professor E.C. Crittenden 61Ct Department of Physics and Chemistry Naval Postgraduate School Monterey, California 93940	2
5.	Lieutenant Colonel, Chang-Hyun Park Republic of Korea Army Military Apartment 3-506, Nam-Hyun Dong, Kawn-Ak Gu, Seoul, Korea	1
6.	Lieutenant Colonel, Yong-Bok Lee Republic of Korea Army 128-5, Pildong, Choong Gu, Seoul, Korea	1